



Article

Development of a Flywheel Hybrid Power System in Vehicles without the Electric Drive Device Rated Capacity Limit

Hong Li ¹, Jiangwei Chu ^{1,*} and Shufa Sun ²

¹ School of Traffic and Transportation, Northeast Forestry University, Harbin 150040, China; lihong9012@163.com

² College of Engineering and Technology, Northeast Forestry University, Harbin 150040, China; ssfangel@163.com

* Correspondence: cjw_62@nefu.edu.cn

Abstract: At present, most studies are focused on converting the vehicle kinetic energy into electrochemical energy for battery storage. During each deceleration period, the kinetic energy is first converted into electromagnetic energy and then stored in the chemical form before being released as the kinetic energy in next acceleration period, which leads to a low transmission efficiency. Secondly, the efficiency of the kinetic energy recovery is limited by the rated capacity of electric drive devices. Thirdly, a single-axis front-drive electric powertrain can only recover the kinetic energy of front wheels. The system proposed in this paper, which included a flywheel, an electromagnetic coupler, and two gear pairs, was arranged in the rear axis. This new configuration could recycle the kinetic energy of the rear wheels for front-driving vehicles. Most of the energy between the wheels and the flywheel was transmitted in the form of mechanical energy, and the power transmitted by the mechanical port of the electromagnetic coupler was not limited by its rated power. Moreover, the battery only needs to recover the slip power of the coupler. Finally, a test bench based on the proposed system was designed and built under deceleration and cruising conditions. The experimental results also proved the functionality of the proposed system.



Citation: Li, H.; Chu, J.; Sun, S. Development of a Flywheel Hybrid Power System in Vehicles without the Electric Drive Device Rated Capacity Limit. *World Electr. Veh. J.* **2022**, *13*, 27. <https://doi.org/10.3390/wevj13020027>

Academic Editor: Joeri Van Mierlo

Received: 17 December 2021

Accepted: 20 January 2022

Published: 21 January 2022

Publisher's Note: MDPI stays neutral with regard to jurisdictional claims in published maps and institutional affiliations.



Copyright: © 2022 by the authors. Licensee MDPI, Basel, Switzerland. This article is an open access article distributed under the terms and conditions of the Creative Commons Attribution (CC BY) license (<https://creativecommons.org/licenses/by/4.0/>).

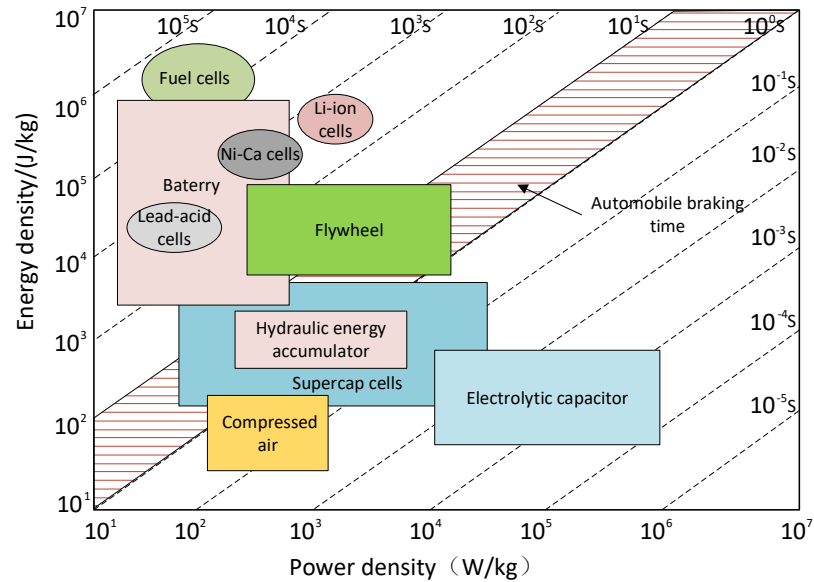
Keywords: flywheel; hybrid power system; electromagnetic coupler; mechanical power; rated capacity

1. Introduction

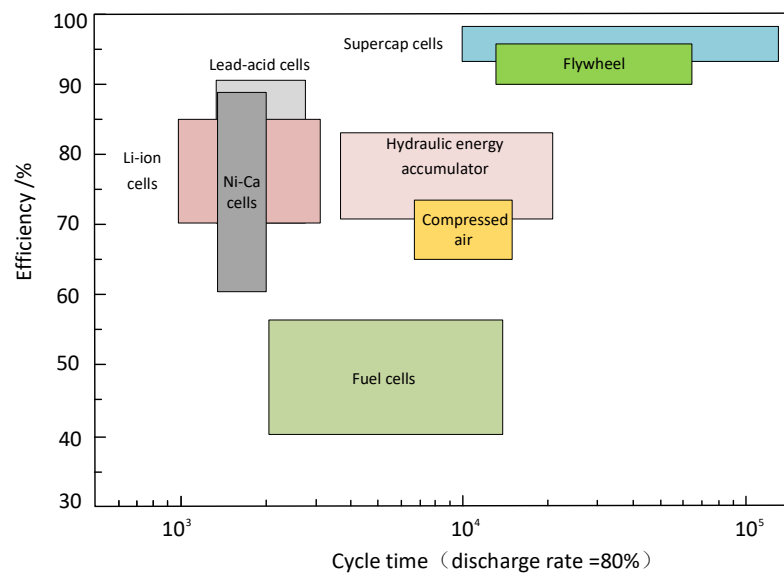
The loss of the vehicle braking energy accounts for approximately 10–30% of the total energy consumption in urban driving conditions [1–3], and braking energy recovery devices can convert part of the vehicle kinetic energy into mechanical energy or electrochemical energy for recovery and storage [4–6]. To date, most studies have focused on converting the kinetic energy of vehicle braking into electrochemical energy, recovering and storing part of the braking energy through motor batteries [7,8]. When the vehicle kinetic energy is recovered and stored in the form of electric energy, the energy conversion process is from mechanical energy to electromagnetic energy and then to chemical energy. The energy conversion amount is limited by the rated capacity of the electric drive device. In particular, when the auxiliary electric drive device is equipped with a low power, the recovery efficiency of the braking energy is lower.

The flywheel hybrid system can satisfactorily solve this problem by combining advanced gearbox control technologies, such as continuously variable transmission (CVT) and Electronic Continuously Variable Transmission (E-CVT), to leverage the higher power density of the flywheel. Typical energy storage technologies include physical energy storage (such as pumped storage energy, compressed air energy storage, and flywheel energy storage), chemical energy storage (such as batteries, fuel cells, liquid flow batteries, and ultracapacitors), and electromagnetic energy storage (such as superconducting electromagnetic energy storage) [9–13]. A fuel cell is not an energy storage, but an energy converter from chemical to electrical energy. The energy is stored in a fuel tank. An energy storage

features energy flow in both directions. However, the energy conversion in the fuel cell is not reversible due to thermodynamical reasons. The characteristics of each energy storage technology are shown in Figure 1.



(a)



(b)

Figure 1. Comparison of the energy storage characteristics of energy storage devices: (a) Ragone plots; and (b) the efficiency-cycle time relationships.

The Ragone plot can be used to evaluate the initial power density and the energy density of the energy storage device; then, the discharge time is defined according to the ratio of the energy density to the power density [14–16], as shown by the imaginary diagonal in Figure 1a. The durations of the charge and the discharge on each imaginary diagonal are equal. In addition, the energy efficiency and the expected number of cycles can also be used to evaluate the energy storage characteristics of the energy storage device. As shown in Figure 1b, when the discharge depth is 80%, the energy efficiencies of the supercapacitor and the flywheel can reach 95%, and the number of cycles exceeds 10,000. Meanwhile, the energy efficiency of the battery is approximately 60–90%, and the number of cycles is 1000–4000. Fuel cells have a low energy efficiency, but a relatively long cycle

life [17,18]. At present, batteries and supercapacitors, as the mainstream energy storage devices for vehicles, can meet the energy needs of vehicles under different working conditions, but these technologies cannot simultaneously consider the power density and energy density requirements. The flywheel can meet the above requirements with relatively high energy density and power density values, and the cycle life and the energy efficiency are higher [19–21].

In October 2009, the Federation Internationale de l'Vehicule (FIA) pointed out the important of the use of flywheel hybrid systems in vehicles. The UK's "Technology Strategy Committee" has also sponsored three research projects on flywheel hybrid systems, which mastered a large number of advanced technologies. In December 2011, the U.S. Department of Energy commissioned Oak Ridge National Laboratory to evaluate flywheel hybrid power systems and pointed out that this technology, with high specific power and energy storage characteristics, has a great potential application in hybrid electric vehicles [22–24]. In 2013, Volvo tested its flywheel kinetic energy recovery system for vehicles, and the results showed that the system could reduce the fuel consumption by 25% [25]. The literature [26] proposed a novel power-split flywheel hybrid system, integrating the CVT and three planetary gear-sets with the flywheel to improve the fuel economy and acceleration performance. HAIKE proposed a recycling kinetic energy propulsion system in the powertrain of a clean energy vehicle, of which the kinetic energy is recovered and stored in a flywheel when braking. When the vehicle is under acceleration, the energy stored in the flywheel is released as a power assistance to enhance the vehicle power performance and reduce the fuel consumption [27]. In reference [28], the zero-inertia power system developed by Eindhoven University of Technology can effectively avoid the acceleration resistance caused by the engine inertia during acceleration.

Based on the electromagnetic coupler and the high efficiency of the flywheel energy storage system, an electromagnetic coupling flywheel energy storage system (ECFESS) was designed. This system effectively solves the insufficient power and energy-saving problem caused by the power limitation of the electric powertrain system in EVs. In addition, the mechanical power of the flywheel can be directly coupled to the powertrain system, which improves the regenerative energy recovery efficiency and the vehicle acceleration performance greatly.

The main contributions of this paper are summarized as follows:

- We proposed a new type of electromagnetic coupling flywheel energy storage system. The proposed topology can improve the performance of front-driving electric vehicles, especially in stopping and going driving.
- Most of the energy between the wheels and the flywheel is transmitted in the form of mechanical energy during the vehicle deceleration and cruising in the proposed system, and the power transmitted by the mechanical port of the electromagnetic coupler is not limited by the rated power.

2. System Modelling

2.1. Working Principle of the ECFESS

The structure of the ECFESS is shown in Figure 2. The braking deceleration process of internal combustion engine vehicles is usually completed by wheel-end friction braking, but that of electric vehicles is completed jointly by friction braking and motor braking, which is the foundation of energy recovery. Compared with that of internal combustion engine vehicles, the use times of the friction braking of electric vehicles are greatly reduced. In most cases, only motor braking can meet the deceleration requirements, and the brake energy required by friction braking is reduced. When the braking torque provided by the driving motor of the front axle or the electromagnetic coupler of the rear axle cannot meet the driver's braking requirement, the remaining braking force is provided by friction braking. Of course, this involves the brake-by-wire system and electro-hydraulic compound-braking mode. In order to highlight the advantage that the power transmitted in the ECFESS is not limited by its rated capacity, only the motor braking mode is discussed.

As an auxiliary device of the electric powertrain system, the proposed system uses an electromagnetic coupler to convert mechanical energy to mechanical energy and mechanical energy to electromagnetic energy and then to chemical energy, when the vehicle decelerates. The energy conversion process is as follows:

- Mechanical energy to mechanical energy conversion process: If the speeds of the armature and magnetic shafts are equal, there is only a mechanical energy conversion between the flywheel and the wheels, without the electromagnetic energy conversion between the battery and the electromagnetic coupler.
- Mechanical energy to electromagnetic energy and then to chemical energy conversion process: If the speeds of the armature shaft and the magnetic shaft are not equal, then part of the mechanical energy is converted between the flywheel and the wheels, and part of the mechanical energy is transmitted through the electrical port of the electromagnetic coupler and stored in the battery. A more detailed discussion on this can be found in Section 2.3.

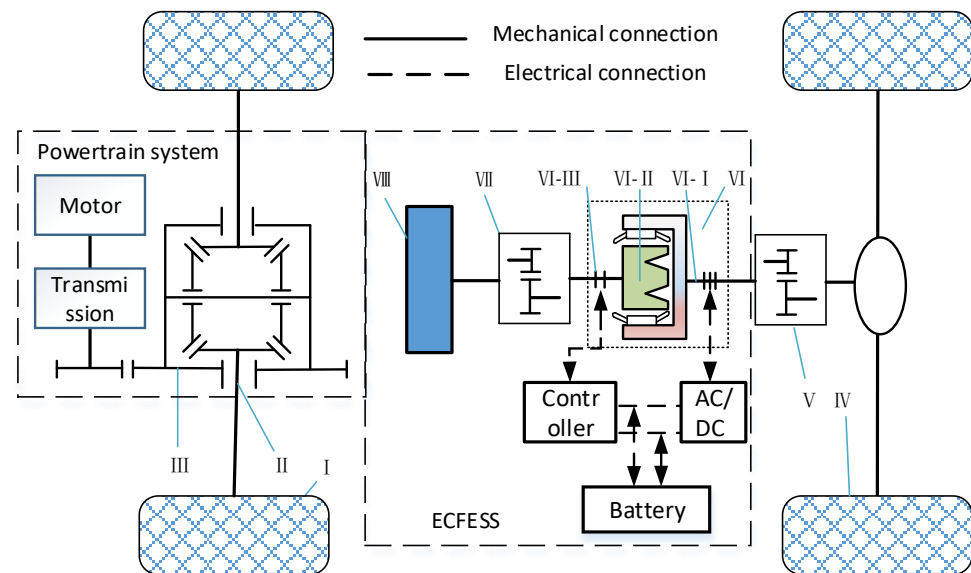


Figure 2. Electromagnetic coupling flywheel energy storage system (ECFESS)-based powertrain system. I—front wheel; II—half-shaft; III—final drive; IV—rear wheel; V—first gear pair; VI—electromagnetic coupler; VI-I—armature shaft (mechanical port); VI-II—magnetic shaft (mechanical port); VI-III—electrical port; VII—second gear pair; VIII—flywheel.

2.2. Characteristics of the ECFESS

The electromagnetic coupler, consisting of two mechanical ports (VI-I and VI-II) and one electrical port (VI-III), was arranged between the flywheel and the wheels, as shown in Figure 2. One mechanical port connected to the rear wheels, and the others connected to the flywheel, so the kinetic energy could transfer from one side to the other. The electromagnetic coupler obeyed the same electromagnetic principles applied to conventional electric machines. The armature, as the outer rotor, and the magnetic pole, as the inner rotor, were embedded with three-phase windings and excitation windings, respectively. The energy recovery device was composed of an AC/DC lift voltage rectifier, a battery (supercapacitor), and a controller, which was used to recover the slip power generated in the armature. The controller was used to adjust the current in the field winding, as well as the output control signal sent to the AC/DC lift voltage rectifier. When the current flow into the rotating magnetic pole winding, the main rotating magnetic field induced a three-phase alternating current in the three-phase winding of the armature. The alternating current was converted into a direct current by the AC/DC lift voltage rectifier and charged into a supercapacitor to realize the recovery of slip power.

When the vehicle decelerated, the kinetic energy was stored in the flywheel through a two-stage gear pair. In the process of energy recovery, the conversion of the mechanical energy between the wheels and the flywheel was realized by controlling the electromagnetic coupler, and the amount of consumed electric energy was far less than the total energy generated in the process of mechanical energy conversion.

To accurately explain the characteristics of the ECFESS, the rotation speeds of the magnetic shaft and the armature shaft are defined as n_i and n_o , respectively, the slip speed and slip power are Δn and P_s , respectively, and the rated speed, rated power, and rated torque of the electromagnetic coupler are n_N , P_N , and T_N , respectively. The rated speed, torque, and power of the electromagnetic coupler obeyed the following equations [29,30]:

$$\Delta n = n_o - n_i, \quad (1)$$

$$P_N = \frac{T_N n_N}{9550}. \quad (2)$$

Assuming that $n_i = i n_N$, $n_o = (i + 1) n_N$, where i is positive, then the output power of the magnetic shaft was written as:

$$P_i = \frac{i T_N n_N}{9550}. \quad (3)$$

The input power of the armature shaft was described as:

$$P_o = \frac{(i + 1) T_N n_N}{9550}. \quad (4)$$

The slip power was written as:

$$P_s = |P_o - P_i| = P_N. \quad (5)$$

The slip speed was expressed as:

$$\Delta n = n_o - n_i = n_N. \quad (6)$$

According to Equations (5) and (6), if the electromagnetic coupler is working under the rated condition and i is positive, the power transmitted by mechanical port is far greater than its rated power and is not affected by the rated power.

The performance evaluation of the flywheel energy storage system is directly related to energy storage efficiency, which means that the whole process of system operation is expected to maximize the available energy, that is, to minimize the energy loss. The flywheel energy storage system is a comprehensive system, bearing friction, windage friction, electrical loss, etc., and will affect the energy utilization efficiency of the system. The flywheel rotor designed in this paper had a maximum speed of 20,000 rpm. In order to reduce the sealing cost, the flywheel worked in the atmospheric environment. Figure 3 shows the wheel–wheel energy conversion efficiency of the ECFESS and the battery electric vehicle.

The technical scheme and the wheel–wheel energy conversion efficiency of the battery electric vehicle (BEV) are shown in Figure 3a,b, respectively. Meanwhile, the ECFESS technical scheme and the energy recovery flow are presented in Figure 3c,d, respectively. The efficiency value for the electrical–mechanical energy conversion was assumed to be 80% [31], which is consistent with the reference in Figure 3b. In general, the transmission efficiency of grade 8 cylindrical gears is 0.97, that of steel bearings is 0.99, and that of elastic coupling is 0.995. In the ECFESS, approximately 30% of the original vehicle kinetic energy was converted to the form of electrical energy, and the rest was transferred mechanically to the buffer flywheel without energy conversion. Figure 3b,d shows that the conversion efficiency of the wheel–wheel kinetic energy of the ECFESS was higher than that of the battery electric vehicle. As we know, due to the limitation of the powertrain capacity of battery electric vehicles, some kinetic energy may be consumed through friction braking and cannot be recovered in the high braking strength requirement or emergency braking

condition. In this case, the advantages of the powertrain system proposed in this paper became prominent.

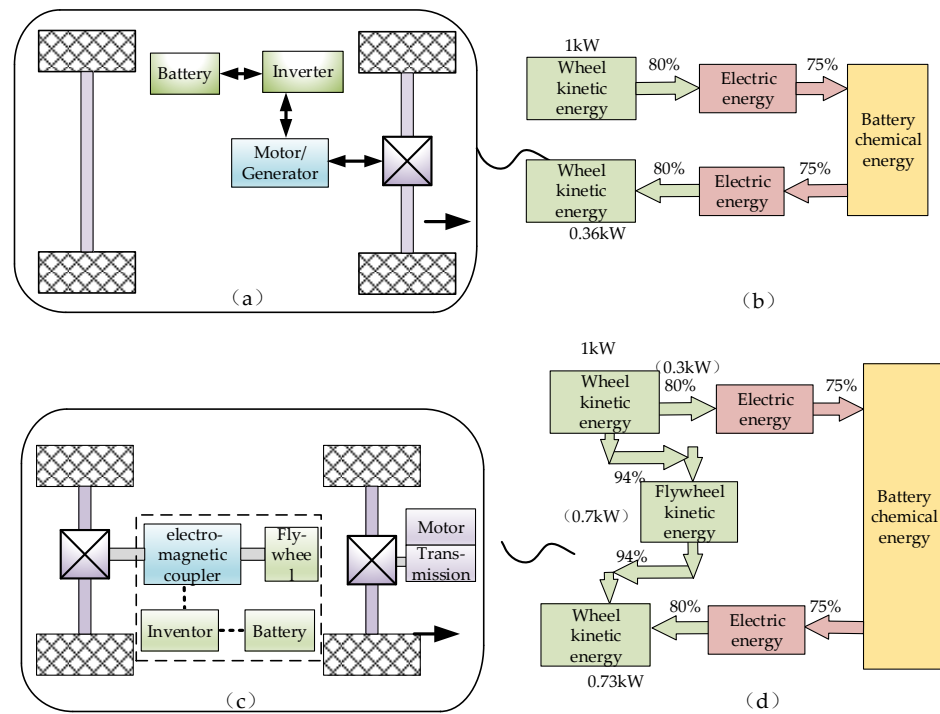


Figure 3. Wheel–wheel energy conversion efficiency: (a) BEV technical scheme; (b) BEV electric powertrain energy conversion efficiency; (c) ECFESS technical scheme; (d) ECFESS energy conversion efficiency.

2.3. Energy Conversion Process Analysis

Under the condition of the vehicle deceleration, part of the vehicle kinetic energy was stored in the flywheel after increasing through the half-shaft, differential, first gear pair, armature shaft, magnetic shaft, and second gear pair.

To describe the energy conversion in the process of the vehicle deceleration in detail, it was assumed that the active power transferred to the armature shaft is P_1 . After deducting the armature iron loss, the electromagnetic power transferred to the magnetic shaft of the electromagnetic coupler through the air gap is P_{em} . The electromagnetic power is divided into the mechanical power P_{emch} and the slip power P_s [30], which can be written as:

$$P_{emch} = (1 - s)P_{em}, \tag{7}$$

$$P_s = sP_{em}, \tag{8}$$

where s is the slip ratio. The mechanical power P_{emch} in the magnetic shaft is outputted to the input shaft of the second gear pair after deducting the mechanical loss. After deducting the copper loss and stray loss of the pole winding, the slip power P_s can be stored in the battery.

When the speed of the armature shaft was greater than the speed of the magnetic shaft, the energy conversion process is shown in Figure 4a. The mechanical power of the magnetic shaft, P_{emch} , was stored in the flywheel through the gear pairs, and the slip power, P_s , was stored in the battery. Figure 4b shows the energy conversion process when the armature and the magnetic axis were at the same speed. At this time, the slip power was zero, and the mechanical energy was stored in the flywheel through the two mechanical ports of the electromagnetic coupler.

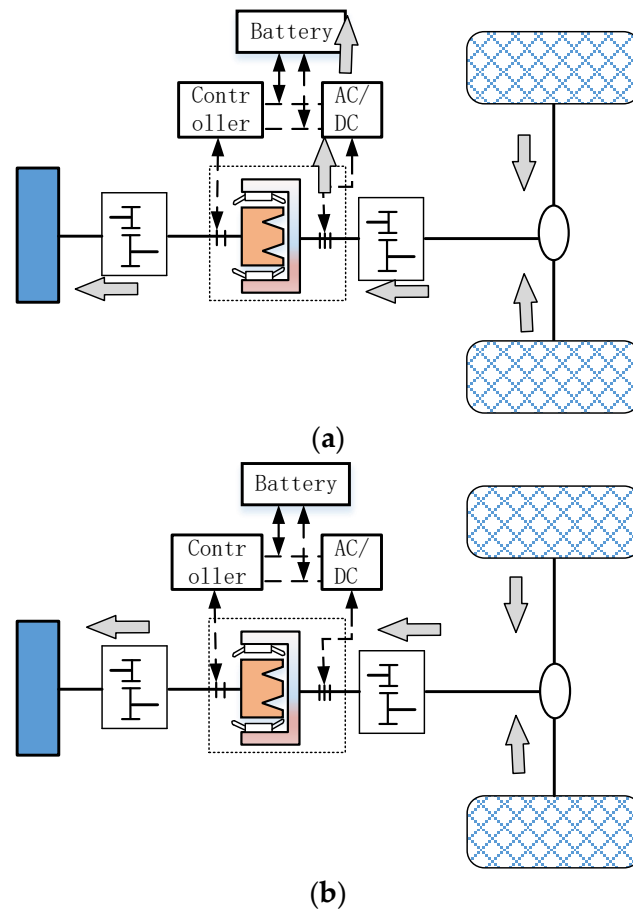
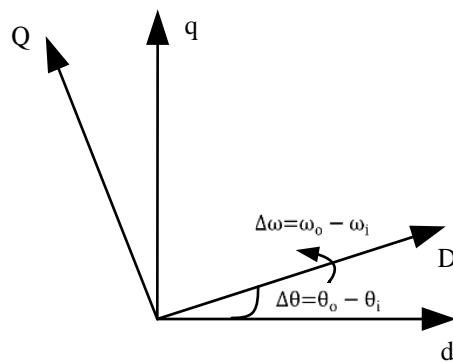


Figure 4. Energy conversion process of the ECFESS: (a) $n_o > n_i$; (b) $n_o = n_i$.

2.4. Characteristic Analysis of the Electromagnetic Coupler

2.4.1. Electromagnetic Coupler Model

The working principle of the electromagnetic coupler is similar to that of the winding AC motor [32,33]. The difference is that the rotating magnetic field of the AC motor is generated by an alternating current, while the magnetic field of the electromagnetic coupler is generated by a direct current. The rotation of the armature plays the role of a rotating magnetic field. Figure 5 shows the coordinate system of the magnetic pole and the armature of the electromagnetic coupler on the dq axis, and its mathematical model can be written as follows [33,34].



$\Delta\theta$ -magnetic pole and armature frame position

Figure 5. dq axis coordinate system of the electromagnetic coupler.

1 Voltage equation

$$\begin{cases} u_{oq} = R_r i_{oq} + \dot{\psi}_{oq} + (\omega_o - \omega_i) \psi_{od} \\ u_{od} = R_r i_{od} + \dot{\psi}_{od} - (\omega_o - \omega_i) \psi_{oq} \end{cases}, \quad (9)$$

where u_{od} and u_{oq} represent the components of the armature winding voltage on the dq axis, R_r represents the resistance of the armature winding, i_{od} and i_{oq} represent the components of the armature winding current on the dq axis, ψ_{od} and ψ_{oq} represent the components of the armature winding flux chain on the dq axis, ω_i represents the electric angular velocity of the magnetic shaft, and ω_o represents the electric angular velocity of the armature shaft.

2 Flux equation

$$\begin{cases} \psi_{od} = L_m i_f + L_{od} i_{od} \\ \psi_{oq} = L_{oq} i_{oq} \end{cases}, \quad (10)$$

where L_{od} and L_{oq} represent the self-inductance components of the armature winding on the dq axis, L_m represents the mutual inductance between the magnetic and armature shafts equivalent windings in the dq coordinate system, and i_f represents the excitation current of the magnetic pole.

3 Electromagnetic torque

$$T_e = 1.5p(\psi_{od}i_{oq} - \psi_{oq}i_{od}), \quad (11)$$

where T_e represents the electromagnetic torque, and p represents the number of pole pairs.

4 Mechanical equations

$$\dot{\omega}_m = \frac{1}{H}(T_e - B\omega_m - T_L), \quad (12)$$

where ω_m represents the mechanical angular velocity of the magnetic shaft, H represents the inertia of the magnetic pole, T_L represents the magnetic pole mechanical torque, and B represents the friction coefficient.

2.4.2. Characteristics

To analyze the dynamic characteristics of the electromagnetic coupler quantitatively, a model of the electromagnetic coupler was established in MATLAB/Simulink according to Equations (9)–(12). The model parameters are shown in Table 1.

Table 1. Model parameters of the electromagnetic coupler.

Parameter	Value
Resistance of the armature winding (Ω)	0.55
Mutual induction of the pole and armature windings (mH)	20
Armature winding d-axis self-induction (mH)	8.45
Armature winding q-axis self-induction (mH)	5.4
Magnetic pole viscous damping ($\text{N}\cdot\text{m}\cdot\text{s}\cdot\text{rad}^{-1}$)	0.22
The moment of inertia of the poles ($\text{kg}\cdot\text{m}^2$)	0.009
Number of pole pairs	3
Excitation nominal voltage (V)	24

The moment of inertia of the poles ($\text{kg}\cdot\text{m}^2$)

By substituting Equation (10) into Equation (11), the electromagnetic torque of the electromagnetic coupler can be obtained:

$$T_e = 1.5p[(L_{od} - L_{oq})i_{oq}i_{od} - L_m i_f i_{oq}]. \quad (13)$$

According to Equation (13), assuming the structural parameters of the electromagnetic coupler are certain, the electromagnetic torque is directly related to i_{od} , i_{oq} , and i_f . If i_f is set as a constant, then Figures 6 and 7 show the characteristics of the electromagnetic torque and the load torque, with the speed difference between the armature and magnetic shafts under no load.

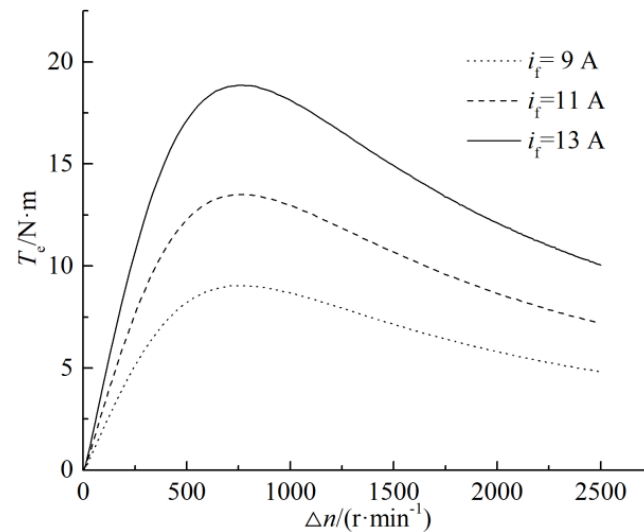


Figure 6. Curves of the speed difference-electromagnetic torque relationships.

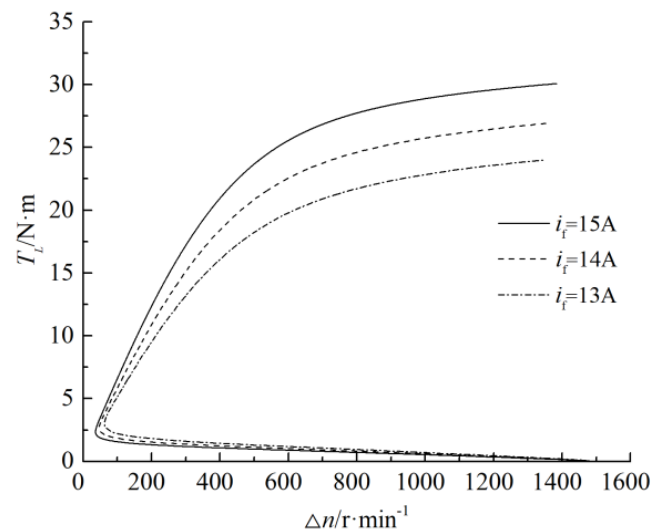


Figure 7. Curves of the speed difference-load torque relationships.

In Figure 6, when the excitation current was constant, the electromagnetic torque first increased and then decreased as the speed difference between the armature and the magnetic shaft increased. Under the same speed difference, the electromagnetic torque increased, as the excitation current increased. If the input speed of the armature shaft was constant, the output speed of the magnetic shaft fluctuated greatly as the load torque changed.

Figure 7 shows the relationship between the load torque and the speed difference between the armature and magnetic shafts under different excitation currents. For $n_o = 1500 \text{ r}\cdot\text{min}^{-1}$, then n_i decreased, as the load torque increased under the same excitation current. Taking $\Delta n = 400 \text{ r}\cdot\text{min}^{-1}$ as an example. When i_f was 15 A and T_L was 20.97 N·m, the magnetic shaft steady speed was $1100 \text{ r}\cdot\text{min}^{-1}$. If the excitation current was reduced to 14 A, the load torque was 18.43 N·m when the magnetic shaft was stable at

1100 r·min⁻¹. The load torque decreased to 16.29 N·m along with the excitation current decreasing to 13 A.

To further study the dynamic output characteristics of the magnetic shaft with the input speed of the armature shaft under different excitation currents, Figure 8 emulates the relationship between the speeds of the magnetic shaft and the armature shaft under a load torque of 6 N·m.

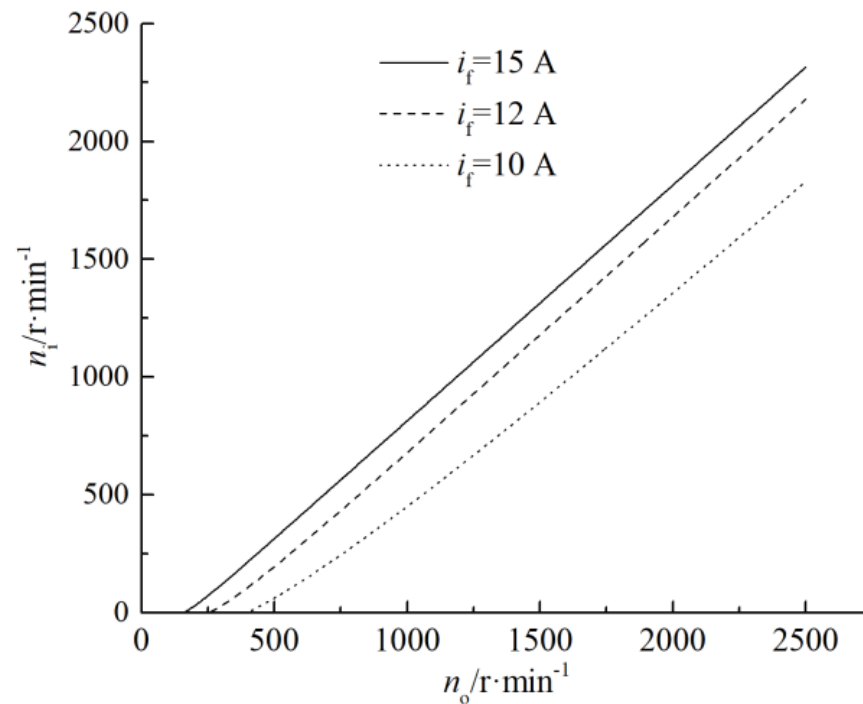


Figure 8. Curves of the input-output speeds.

In Figure 8, the output speed of the magnetic shaft increased linearly, as the input speed increased at a certain constant excitation current. When the excitation current was 15 A, the sum of the load torque and the friction torque was greater than the electromagnetic torque when the input speed of the armature was lower than 161 r·min⁻¹, and the output speed of the magnetic shaft was zero. When the excitation current was decreased from 12 A to 10 A, the critical speed of the armature was changed from 256 r·min⁻¹ to 397 r·min⁻¹.

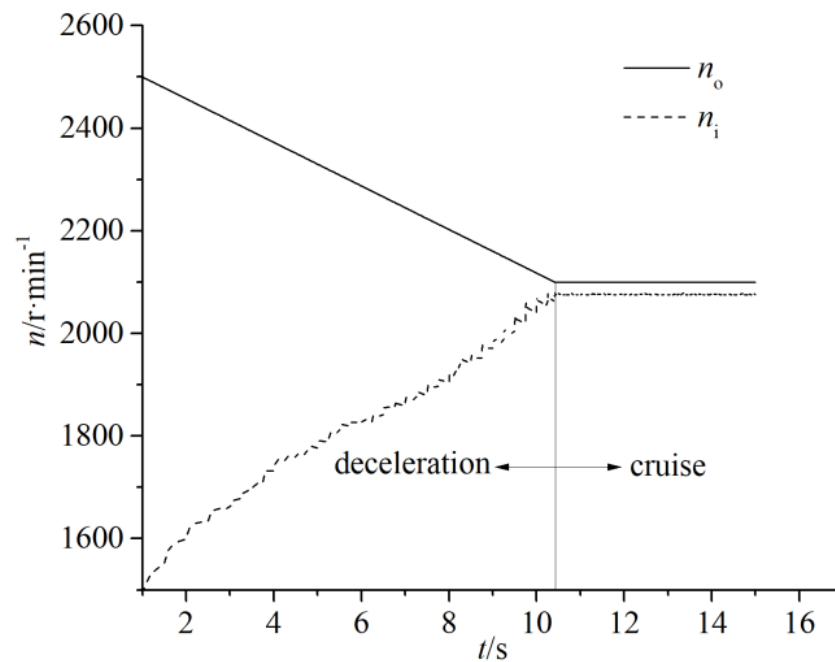
3. Case Study

In this section, the mathematical model of the ECFESS was established based on Figure 2. The parameters are shown in Table 2.

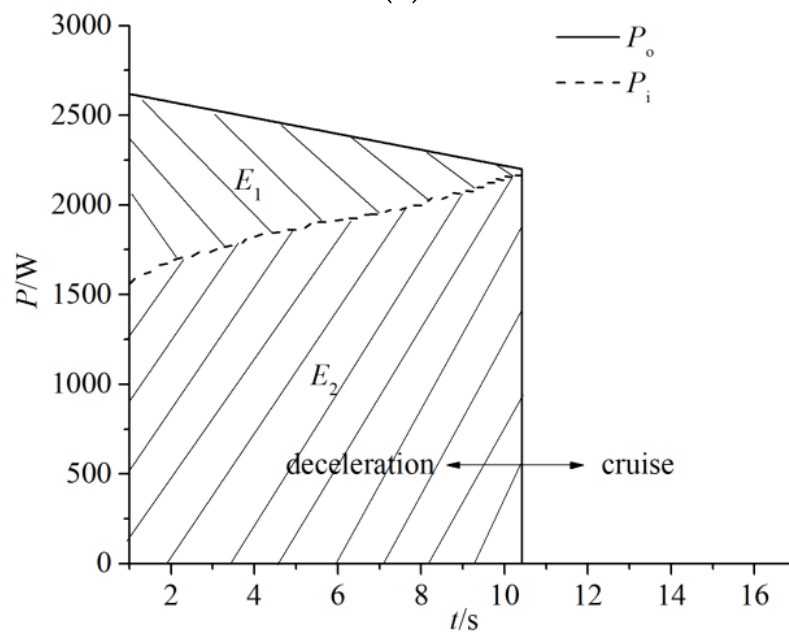
Table 2. Parameters of the ECFESS.

Parameter	Value
Mass (kg)	1500
Wheel radius (m)	0.3
Flywheel inertia/(g·m ²)	0.3
Flywheel maximum speed (r·min ⁻¹)	20,000
Flywheel initial speed (r·min ⁻¹)	7500
First gear pair ratio	1:4
Second gear pair ratio	1:5
Coupler rated power (kW)	1.1
Rated speed (r·min ⁻¹)	1000
Rated torque (N·m)	10

Figure 9a shows the braking energy conversion process when the wheel decelerated from an initial speed of $625 \text{ r}\cdot\text{min}^{-1}$ to a cruising speed of $525 \text{ r}\cdot\text{min}^{-1}$, which means that the vehicle speed changed from $70.69 \text{ km}\cdot\text{h}^{-1}$ to $59.38 \text{ km}\cdot\text{h}^{-1}$. In this process, following the driver's demand, a rated torque of $-10 \text{ N}\cdot\text{m}$ was applied to the mechanical port of the coupler. At $t = 10.42 \text{ s}$, the kinetic energy of the flywheel absorbed from the rear wheel was 177.05 kJ (initial energy: 92.43 kJ). Therefore, the flywheel speed increased from $7500 \text{ r}\cdot\text{min}^{-1}$ to $10,380 \text{ r}\cdot\text{min}^{-1}$.



(a)



(b)

Figure 9. Energy conversion during vehicle deceleration and cruising: (a) speed of the coupler mechanical port; (b) power of the coupler mechanical port.

In Figure 9b, the input power of the armature shaft was 2.62 kW, and the output power of the magnetic shaft was 1.56 kW at $t = 1.00$ s. The output power of the coupler increased from 1.56 kW to 2.20 kW in the period of 1.00–10.42 s. In this process, the power transmitted by the mechanical port of the electromagnetic coupler was greater than its rated power. To explain the energy stored in the battery (supercapacitor) of the ECFESS, the input energy of the electromagnetic coupler E_i and the output energy E_o were defined as follows:

$$\begin{cases} E_i = \int_1^{10.42} P_o dt \\ E_o = \int_1^{10.42} P_i dt \end{cases} \quad (14)$$

Figure 9b shows that the input energy of the electromagnetic couple ($E_i = E_1 + E_2$) was 25.11 kJ and the output energy ($E_o = E_2$) was 19.59 kJ. Therefore, the maximum energy recovered from the battery (E_1) in the deceleration–cruise process was 5.52 kJ. In other words, the ECFESS proposed in this paper could store directly 78.02% of kinetic energy from the rear wheel in the flywheel, and 21.98% of the energy was converted through the electrical port and stored in the battery eventually.

To analyze the energy conversion of the ECFESS quantitatively, Table 3 shows the power transmitted by the mechanical and electrical ports when the wheel speed decreased from 622.5 $\text{r}\cdot\text{min}^{-1}$ to 535 $\text{r}\cdot\text{min}^{-1}$ in the vehicle deceleration status.

Table 3. Power of the coupler ports.

n_o $\text{r}\cdot\text{min}^{-1}$	n_i $\text{r}\cdot\text{min}^{-1}$	P_o (kW)	P_i (kW)	P_s (kW)	$\frac{P_s}{P_o}$
2490	1533	2.608	1.605	1.003	0.385
2465	1595	2.581	1.670	0.911	0.353
2440	1634	2.555	1.710	0.845	0.331
2415	1659	2.529	1.737	0.792	0.313
2390	1707	2.503	1.787	0.716	0.286
2365	1753	2.477	1.836	0.641	0.259
2340	1769	2.451	1.853	0.598	0.244
2315	1809	2.424	1.894	0.530	0.219
2290	1826	2.398	1.912	0.486	0.203
2265	1857	2.372	1.944	0.428	0.180
2240	1874	2.346	1.962	0.384	0.164
2215	1894	2.320	1.983	0.377	0.163
2190	1949	2.293	2.041	0.252	0.110
2165	1972	2.267	2.065	0.202	0.089
2140	1998	2.241	2.093	0.148	0.066

In Table 3, the output power P_i of the electromagnetic coupler increased from 1.605 kW to 2.093 kW in the process of decreasing, and the transmitted power was approximately 1.46–1.90 times of the rated power. The slip power P_s processed by the electrical port was reduced rapidly from 1.003 kW to 0.148 kW, and the ratio of the slip power to the input power of the armature was reduced from 38.5% to 6.6%. According to the above data variation rules, the proposed system can convert most of the kinetic energy in the process of braking deceleration into mechanical energy, and the amount of energy conversion is not limited by the rated capacity of the electromagnetic coupler.

4. Experimental Results

For the proof of the concept, an ECFESS test bench was designed and tested. The experimental information is shown in Figure 10 and Table 4. Flywheel I and flywheel II were connected to a mechanical port by V-belts. Flywheel II could simulate the initial energy of a decelerating condition at a certain speed. The energy from wheels could be directly stored in flywheel I in the form of mechanical energy through a first-stage V-belt, an electromagnetic coupler, and a second-stage V-belt.

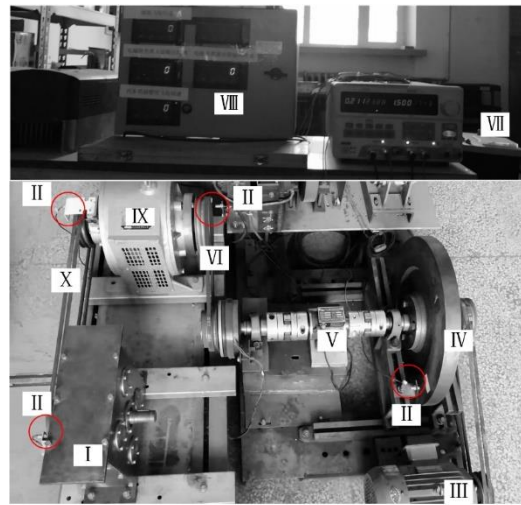


Figure 10. ECFESS test bench. I—flywheel I; II—speed sensor (red circle); III—motor; IV—flywheel II; V—torque sensor; VI—first-stage V-belt; VII—controller; VIII—data collection system; IX—electromagnetic coupler; X—second-stage V-belt.

Table 4. Experimental parameters of the ECFESS.

Electromagnetic Coupler Parameters	
Excitation voltage (V)	<90
Excitation current (A)	<1.8
Rated power (kW)	4.0
Rated speed ($\text{r}\cdot\text{min}^{-1}$)	1528
Rated torque (N·m)	25
Number of pole pairs	3
Drive motor parameters	
Rated voltage (V)	220
Rated current (A)	8.29
Rated power (kW)	4.0
Rated speed ($\text{r}\cdot\text{min}^{-1}$)	2890
Rated torque (N·m)	13.2
Flywheel inertias ($\text{kg}\cdot\text{m}^2$)	
Flywheel I	2.99
Flywheel II	4.82
V-belt speed ratio	
First-stage V-belt	1:1.35
Second-stage V-belt	1:1.28

In this scenario, as shown in Figure 11a, flywheel II had an initial speed of $702 \text{ r}\cdot\text{min}^{-1}$, while flywheel I's speed was zero at the beginning. Meanwhile, a negative torque equal to $25 \text{ N}\cdot\text{m}$ was applied to coupler's mechanical port (armature shaft and magnetic shaft), until the speed of the mechanical port was about the same. The process ended at $t = 5.72 \text{ s}$ when cruising. Figure 11b shows the power of the coupler mechanical port. During the process, the power of armature shaft reduced from 1.85 kW to 1.27 kW . Therefore, a power of 8.93 kJ was input into the coupler, while a power of 4.81 kJ was directly output to flywheel I in the form of mechanical energy. Therefore, the maximum energy required for battery processing was 4.1 kJ in the form of chemical energy.

If the magnetic shaft of the coupler was locked, the coupler was equal to a generator. In the same situation, flywheel II also had an initial speed of $702 \text{ r}\cdot\text{min}^{-1}$, while a negative torque equal to $25 \text{ N}\cdot\text{m}$ was applied to the coupler's armature shaft. The same was true for

an 8.93 kJ input into the coupler. However, all this required the battery to process in the form of chemical energy.

In order to illustrate the power characteristics of the system furtherly, we increased the input speed of the electromagnetic coupler to obtain the results in Figure 12. Figure 12a shows that at $t = 2.09$ s, the electromagnetic coupler mechanical ports rotated at the rates of $1904 \text{ r}\cdot\text{min}^{-1}$ and $259 \text{ r}\cdot\text{min}^{-1}$ in the same direction. At this moment, the flywheel II was powered off, and a $25 \text{ N}\cdot\text{m}$ torque was generated by the electromagnetic coupler. For $t = 8.49$ s, the magnetic shaft speed increased to $1561 \text{ r}\cdot\text{min}^{-1}$ due to the electromagnetic torque, while the input speed decreased to $1621 \text{ r}\cdot\text{min}^{-1}$. In this process, the input power of the electromagnetic coupler was reduced from 4.983 kW to 4.243 kW , while the output power was increased from 0.678 kW to 4.085 kW . Therefore, the power transmitted by the coupler was greater than its rated power. The maximum recoverable energy of the battery in the vehicle deceleration–cruise condition was 14.281 kJ , i.e., E_1 in Figure 12b. Under the same deceleration–cruise condition, the BEV needed to convert 29.523 kJ from the rotor shaft to electrochemical energy, which was stored in the battery. That is, the ECFESS proposed in this paper can be of importance to chemical batteries by reducing the power demand as well as the depth of charge and discharge.

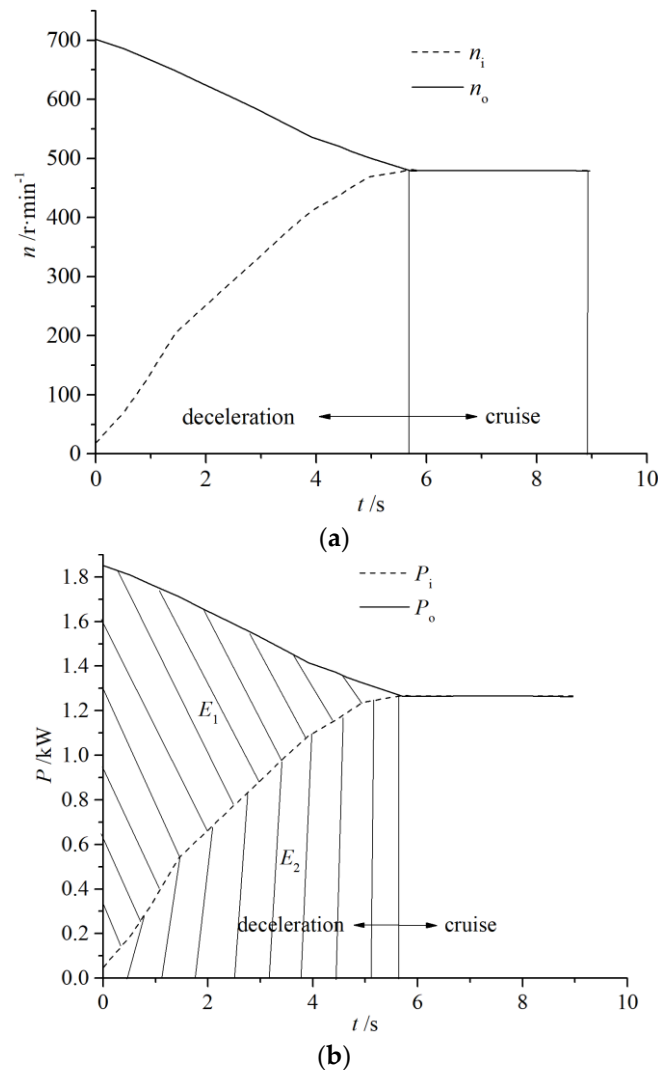


Figure 11. Experimental results of lower power transmission: (a) electromagnetic coupler mechanical port speed; (b) electromagnetic coupler mechanical port power.

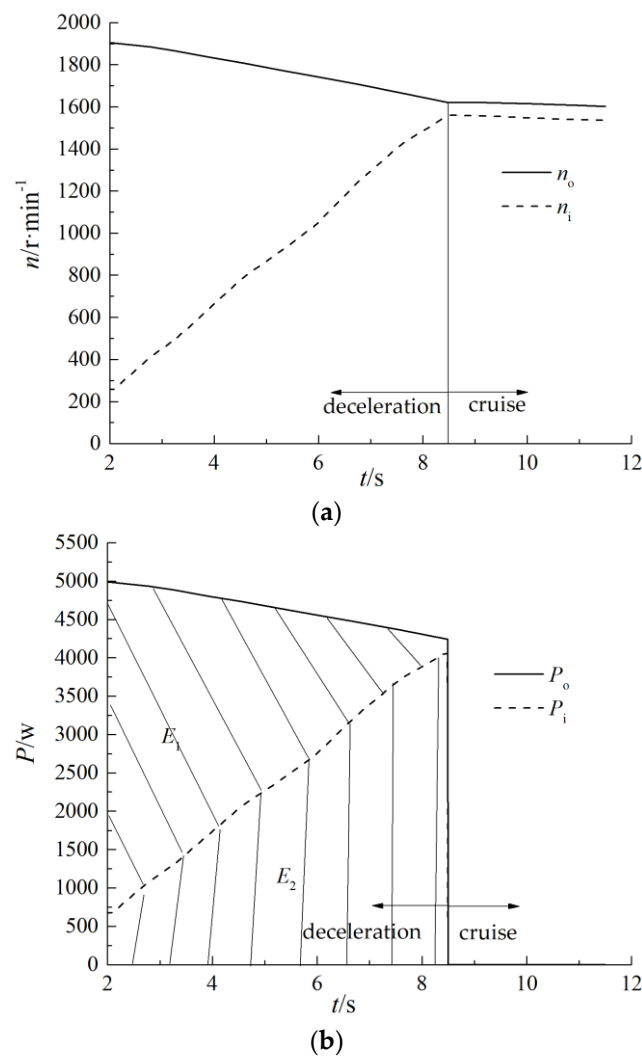


Figure 12. Experimental results of high power transmission: (a) electromagnetic coupler mechanical port speed; (b) electromagnetic coupler mechanical port power.

5. Conclusions

The hybrid vehicle technology is a well-conceived method of improving the efficiency and quality of operation of vehicles. To meet requirements for hybrid powertrains, advanced high power energy storage and conversion technologies are needed. These technologies should address issues of high power energy storage, energy/power management, and auxiliary power. Advanced flywheel high power energy storage systems are one possible way to meet high power energy storage and energy/power conversion needs.

In this paper, a new-type energy storage system, the ECFESS, was proposed based on the high efficiency of flywheel energy storage and the characteristics of electromagnetic couplers. The ECFESS was arranged on the rear axle of a vehicle, which can recover part of the rear axle braking energy. Then, the electromagnetic coupler model was modelled in MATLAB/Simulink, and the characteristics of this model were analyzed. In the deceleration state, the ECFESS could store the vehicle kinetic energy in two parts. One part was converted into electrochemical energy and stored in a battery, and the remainder was directly converted into mechanical energy, which improved the brake energy recovery efficiency, especially in stopping and going driving. As the vehicle wheel speed decreased, the power processed by the electrical port of the electromagnetic coupler was much smaller than the power transmitted by the mechanical port. In this way, the conversion power between the battery and the electromagnetic coupler was lower. More importantly, in the process of the vehicle deceleration and cruising, the power transmitted by the mechanical

port was not limited by the rated capacity of the electromagnetic coupler. At the end, an ECFESS test bench has been designed and tested for the proof of the concept.

Author Contributions: Methodology, H.L. and J.C.; software, H.L.; validation, H.L. and S.S.; writing—original draft preparation, H.L.; writing—review and editing, H.L. and J.C. All authors have read and agreed to the published version of the manuscript.

Funding: This research was funded by the National Key Research and Development Program Project of China (Grant No. 2018YFE0207800-04) and the Fundamental Research Funds for the Central Universities of China (Grant No. 2572020AW49).

Institutional Review Board Statement: Not applicable.

Informed Consent Statement: Not applicable.

Data Availability Statement: The data presented in this study are available on request from the corresponding author.

Conflicts of Interest: The authors declare no conflict of interest.

References

- Choi, G.; Jahns, T.M. Design of electric machines for electric vehicles based on driving schedules. In Proceedings of the 2013 International Electric Machines & Drives Conference, Chicago, IL, USA, 12–15 May 2013. [\[CrossRef\]](#)
- Liu, W.; Qi, H.; Liu, X.; Wang, Y. Evaluation of regenerative braking based on single-pedal control for electric vehicles. *Front. Mech. Eng.* **2020**, *15*, 166–179. [\[CrossRef\]](#)
- Berzi, L.; Delogu, M.; Pierini, M. Development of driving cycles for electric vehicles in the context of the city of Florence. *Transp. Res. Part D Transp. Environ.* **2016**, *47*, 299–322. [\[CrossRef\]](#)
- Li, H.; Chu, J.W.; Yuan, S.K. Performance of Vehicle Electromagnetic Coupling Flywheel Energy Storage Device. *J. South China Univ. Technol.* **2020**, *48*, 50–57. [\[CrossRef\]](#)
- Atienza, A.H.; Cariño, A.; Jacinto, N.; Tapia, S. Mechanical Interface of Flywheel Kinetic Energy Recovery System on Motorized Tricycles. *J. Phys. Conf. Ser.* **2020**, *151*, 012001. [\[CrossRef\]](#)
- Li, H.; Chu, J.; Li, J.; Cui, P. Energy recovery characteristic of flywheel energy storage for vehicular applications. *J. Huazhong Univ. Sci. Technol.* **2017**, *45*, 51–57. [\[CrossRef\]](#)
- Dhand, A.; Pullen, K. Review of Flywheel Based Internal Combustion Engine Hybrid Vehicles. *Int. J. Automot. Technol.* **2013**, *14*, 707–804. [\[CrossRef\]](#)
- Li, H.; Zhu, J.; Sun, S.; Li, H. Application progress of the flywheel hybrid powertrain in vehicle. *Energy Storage Sci. Technol.* **2021**, *10*, 534. [\[CrossRef\]](#)
- Amiryar, M.E.; Pullen, K.R. A Review of Flywheel Energy Storage System Technologies and Their Applications. *Appl. Sci.* **2017**, *7*, 286. [\[CrossRef\]](#)
- Sakti, A.; O’Sullivan, F. *Storage, Renewables and the Evolution of the Grid*; MIT Energy Initiative: Cambridge, MA, USA, 2015.
- Editorial Department of China Journal of Highway and Transport. Review on China’s Automotive Engineering Research Progress: 2017. *China J. Highw. Transp.* **2017**, *30*, 1–197.
- Itani, K.; De Bernardinis, A.; Khatir, Z.; Jammal, A. Comparative analysis of two hybrid energy storage systems used in a two front wheel driven electric vehicle during extreme start-up and regenerative braking operations. *Energy Convers. Manag.* **2017**, *144*, 69–87. [\[CrossRef\]](#)
- Hannan, M.A.; Hoque, M.M.; Mohamed, A.; Ayob, A. Review of energy storage systems for electric vehicle applications: Issues and challenges. *Renew. Sustain. Energy Rev.* **2017**, *69*, 771–789. [\[CrossRef\]](#)
- Rufer, A. The Dream of Efficient Energy Storage-From BESS, KERS & Co. to the Hybrid Power Plant. In Proceedings of the 19th European Conference on Power Electronics and Applications (EPE’17 ECCE Europe), Warsaw, Poland, 11–14 September 2017. [\[CrossRef\]](#)
- Christen, T.; Carlen, M.W. Theory of Ragone plots. *J. Power Sources* **2000**, *91*, 210–216. [\[CrossRef\]](#)
- Martine, J.A. Modeling and Characterization of Energy Storage Devices. In Proceedings of the IEEE Power and Energy Society General Meeting, Detroit, MI, USA, 24–28 July 2011. [\[CrossRef\]](#)
- Guney, M.S.; Tepe, Y. Classification and assessment of energy storage systems. *Renew. Sustain. Energy Rev.* **2017**, *75*, 1187–1197. [\[CrossRef\]](#)
- Hannan, M.A.; Azidin, F.A.; Mohamed, A. Hybrid electric vehicles and their challenges: A review. *Renew. Sustain. Energy Rev.* **2014**, *29*, 135–150. [\[CrossRef\]](#)
- Hadjipaschalis, I.; Poullikkas, A.; Efthimiou, V. Overview of current and future energy storage technologies for electric power applications. *Renew. Sustain. Energy Rev.* **2009**, *13*, 1513–1522. [\[CrossRef\]](#)
- Vazquez, S.; Lukic, S.M.; Galvan, E.; Franquelo, L.G.; Carrasco, J.M. Energy Storage Systems for Transport and Grid Applications. *IEEE Trans. Ind. Electron.* **2010**, *57*, 3881–3895. [\[CrossRef\]](#)

21. González-Gil, A.; Palacin, R.; Batty, P. Sustainable urban rail systems: Strategies and technologies for optimal management of regenerative braking energy. *Energy Convers. Manag.* **2013**, *75*, 374–388. [[CrossRef](#)]
22. Hansen, J.G.R.; O'kain, D.U. *An Assessment of Flywheel High Power Energy Storage Technology for Hybrid Vehicles*; Oak Ridge National Laboratory: Oak Ridge, TN, USA, 2012. Available online: <https://info.ornl.gov/sites/publications/Files/Pub31707.pdf> (accessed on 10 June 2021).
23. Changzhou Haike New Energy. *Milestone*; Changzhou Haike New Energy: Changzhou, China, 2012; Available online: <http://www.chk-net.com/product.asp?id=9> (accessed on 8 October 2021).
24. Bolund, B.; Bernhoff, H.; Leijon, M. Flywheel energy and power storage systems. *Renew. Sustain. Energy Rev.* **2007**, *11*, 235–258. [[CrossRef](#)]
25. Volvo Car Group. Volvo Car Group and Flybrid Conduct UK Testing of Flywheel KERS Technology. Available online: <https://www.media.volvocars.com/uk/en-gb/media/pressreleases/141626/volvo-car-group-and-flybrid-conduct-uk-testing-of-flywheel-kers-technology> (accessed on 16 November 2021).
26. Song, C.; Kum, D.; Kim, K.S. Feasibility analysis and performance evaluation of a novel power-split flywheel hybrid vehicle. *Energies* **2018**, *11*, 1744. [[CrossRef](#)]
27. Changzhou Haike New Energy. *Recycling Kinetic Energy Propulsion System—“Electrical Type” Flywheel KERS*; Changzhou Haike New Energy: Changzhou, China, 2012. Available online: <http://www.chk-net.com/product.asp?id=12> (accessed on 15 October 2021).
28. Serrarens, A.F.A.; Shen, S.W.; Veldpaus, F.E. Powertrain control of a flywheel assisted driveline with continuously variable transmission. *J. Dyn. Syst. Meas. Control.* **2003**, *125*, 455–461. [[CrossRef](#)]
29. Fathe, A. *Transformers and Electric Machinery Fundamentals*; LAP Lambert Academic Publishing: 2015. Available online: <https://www.morebooks.de/store/cn/book/transformers-and-electric-machinery-fundamentals/isbn/978-3-659-66951-4> (accessed on 10 July 2021).
30. Tang, T.H. *Fundamentals of Motor and Drive*; China Machine Press: Beijing, China, 2016.
31. Pullen, K.R.; Ellis, C.W.H. Kinetic energy storage for vehicles. In Proceedings of the IET—The Institution of Engineering and Technology Hybrid Vehicle Conference 2006, Coventry, UK, 12–13 December 2006; pp. 91–108. [[CrossRef](#)]
32. Xia, L.; Jiang, H.B.; Geng, G.Q. A Study on Steady-state Performance of Winding Type Permanent Magnet Coupler in W-ECHPS System of a Heavy Vehicle. *Automot. Eng.* **2019**, *41*, 703–710. [[CrossRef](#)]
33. Nasiri, H.; Radan, A.; Ghayebloo, A.; Ahi, K. Dynamic modeling and simulation of transmotor based series-parallel HEV applied to Toyota Prius 2004. In Proceedings of the 10th International Conference on Environment and Electrical Engineering, Rome, Italy, 8–11 May 2011. [[CrossRef](#)]
34. Jiang, H.-B.; Tang, B.; Xu, Z.; Geng, G.-Q. Electromagnetic and Torque Characteristics of Electromagnetic Slip Coupling Applied to Hydraulic Power Steering System for Heavy-Duty Vehicles. *J. Comput. Theor. Nanosci.* **2015**, *12*, 1069–1075. [[CrossRef](#)]